# Olefin-Dependent Discrimination Between Two Nonheme HO-Fe^{V}=O Tautomeric Species in Catalytic H$_2$O$_2$ Epoxidations**

Anna Company, Yan Feng, Mireia Güell, Xavi Ribas, Josep M. Luis, Lawrence Que, Jr. and Miquel Costas*

Nonheme iron oxygenases are emerging as versatile biological catalysts involved in a number of oxidative processes with biomedical, environmental and technologic implications.[1] Their heme counterparts are commonly taken as precedents for their chemistry.[2] In the heme paradigm, O-O heterolytic cleavage of an Fe^{III}-OOH intermediate affords a high valent metal-oxo species that acts as the oxidant for the reaction (Scheme 1). Although nonheme iron oxygenases are less well understood, evidence has accumulated in the last few years that high valent iron-oxo species are also involved in some of their catalytic pathways..[3] Furthermore, a number of synthetic model complexes have been described.[4]

Scheme 1
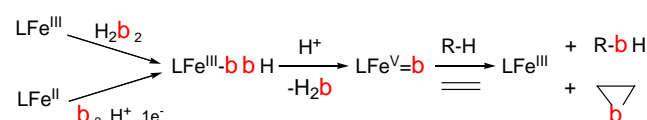
We have recently described that [Fe(OTf)$_2$(^{Me2}PyTACN)] (**1**) (OTf = CF$_3$SO$_3$, Scheme 2) is a stereoselective alkane hydroxylation catalyst in combination with H$_2$O$_2$, and that oxidations occur *via* sole implication of a high valent HO-Fe^{V}=O species.[5] We have also shown that **1** is an excellent olefin oxidation catalyst, affording large turnover numbers (TN) of epoxide and *cis*-diol products with unprecedented efficiency (Scheme 2, bottom).[6,7] Surprising mechanistic insights into these reactions are described in the present work, showing a reaction mechanism that does not conform to the canonical heme oxygenase paradigm.

Mechanistic studies were run under conditions of large excess

[∗]   Dr Miquel Costas, Anna Company, Dr Xavi Ribas
      Departament de Química
      Universitat de Girona
      Campus de Montilivi, E-17071, Girona, Spain
      E-mail: miquel.costas@udg.edu
      Dr Josep M. Luis, Mireia Güell
      Institute of Computational Chemistry
      Universitat de Girona
      Campus de Montilivi, E-17071, Girona, Spain
[*]   Prof. Dr. Lawrence Que Jr., Yan Feng
   Department of Chemistry and Center for Metals in Biocatalysis
      University of Minnesota
      207 Pleasant Str SE Mpls, MN, 55545
      E-mail: larryque@umn.edu

Supporting information for this article is available on the WWW under http://www.angewandte.org or from the author.

of olefin to minimize overoxidation reactions and also due to limitations imposed by the use of isotopically labeled compounds (*vide infra*). All the reactions were run under a N$_2$ atmosphere to avoid autooxidation processes due to the presence of O$_2$. In a typical experiment, 10 equiv of H$_2$O$_2$ (70 mM solution in CH$_3$CN) were delivered by syringe pump together with 1000 equiv of H$_2$O over a period of 30 min into an acetonitrile solution containing 1 equiv of the iron catalyst **1** (final concentration = 1 mM) and the specific alkene (0.05-1 M). In all olefin oxidation reactions explored (Table 1), mixtures of *cis*-diol and epoxide were obtained with modest to excellent efficiency in the conversion of H$_2$O$_2$ into products (3.9 to 8.9 TN, maximum TN = 9.5). The diol:epoxide (D:E) ratio observed in these reactions was dependent on the specific olefin, and it ranges from 3:2 (cyclooctene) to 8:1 (1-octene). Oxidation of *cis*-2-heptene by **1** was highly stereoselective and afforded 3.5 TN of diol (95% *cis*) and 1.8 TN of epoxide (97% *cis*).

Scheme 2.
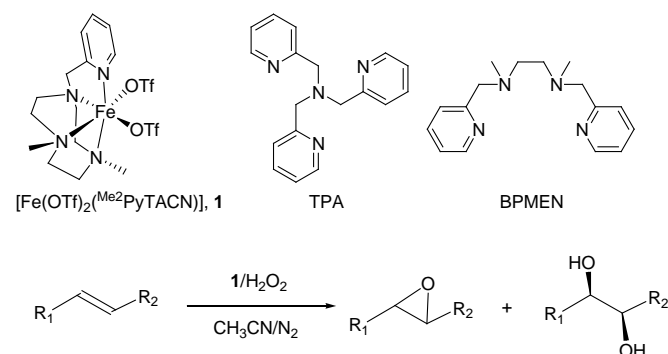
Insight into the olefin oxidation mechanisms was obtained by means of isotopic labeling with H$_2^{18}$O$_2$ and H$_2^{18}$O. Studies of the oxidation of cyclooctene using H$_2^{18}$O$_2$ indicated that only 25% of the oxygen atoms in the epoxide derived from H$_2$O$_2$. Complementary experiments carrying out the oxidation in the presence of H$_2^{18}$O (1000 equiv) showed 61% incorporation of oxygen atoms from water into the epoxide. On the other hand, 84% of the *cis*-diol product contained one oxygen atom derived from H$_2$O$_2$ and one oxygen atom from H$_2$O. Oxidation of cyclooctene under analogous conditions as a function of the amount of H$_2^{18}$O added to the reaction mixture showed that the fractions of labeled epoxide and *cis*-diol increased linearly with [H$_2^{18}$O] at lower concentrations but reached a plateau at higher concentrations (Figure S1), indicative of a saturation behavior. These data strongly implicate a reversible water binding step (scheme 3) prior to the generation of the species responsible for olefin oxidation.[8]

Results of catalytic oxidations of different olefins by **1** in the presence of 1M H$_2^{18}$O (conditions for maximum ^{18}O incorporation) are listed in Table 1. A major fraction of the *cis*-diol products obtained in the oxidation of all the substrates tested contained one oxygen atom

derived from water. This picture is reminiscent of the *cis*-diol labeling patterns observed for [Fe(TPA)(CH$_3$CN)$_2$]$^{2+}$ **2**, and [Fe(BPMEN)(CH$_3$CN)$_2$]$^{2+}$,[8] **3** (Scheme 2), therefore strongly implicating the generation of a HO-Fe^V=O oxidant *via* a water-assisted O-O heterolysis of a H$_2$O-Fe^{III}-OOH species (Scheme 3).[9] Epoxides are formed by transfer of the oxo group to the olefin, while *cis*-diols are formed by transfer of both oxo and hydroxo groups to the double bond.[10]

Scheme 3
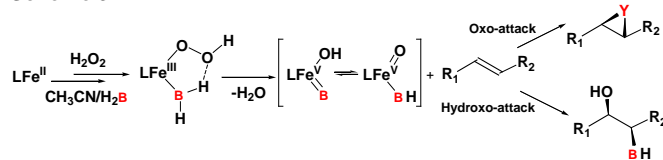
Much more surprising were labeling results for epoxidations catalyzed by **1**, in which all epoxides showed a much higher incorporation of oxygen atoms from water (33-71%) than found for **2** and **3** (Table 1). Indeed, the activity of **1** is unprecedented as water is the main source of oxygen atoms in the epoxidation of most of the substrates studied. In addition, the extent of label incoporation depended on the nature of the olefin. *Cis*-disubstituted, trisubstituted and terminal olefins afforded epoxides with 64±7% of the oxygen from water, while the level of water incorporation in *trans*-disubstituted olefins was 33%. For comparison, epoxidation reactions of *cis*-2-heptene, *trans*-2-heptene and 1-octene catalyzed by **2** and **3** exhibited a level of water incorporation into epoxide products that was substrate independent, 10% for **2** and 21% for **3**. Lastly, because of the high extent of label incorporation observed for **1**-catalyzed epoxidations, the dependence of label incorporation on substrate concentration could be investigated (Table 1). Interestingly, no dependence was found, demonstrating that label exchange must be faster than the substrate oxidation step and does not compete with it.

Table 1. Olefin oxidation reactions catalyzed by iron catalysts **1-3** (1 mM) in the presence of 1 M H$_2$^{18}O under N$_2$.

| Cat	Substrate	cat:Ox:S[a]	D[b]/E[c]	^{16}O^{18}O[d][f]	^{18}O[e][f]
1	1-octene	1:10:1000	8.1/0.8	80	60
1	*trans*-2-octene	1:10:1000	2.6/1.3	73	33
1	*trans*-3-octene	1:10:1000	3.7/1.6	75	33
1	*trans*-4-octene	1:10:1000	3.7/2.1	71	33
1	*cis*-2-heptene	1:10:1000	3.0/1.2	74	60
1	*cis*-2-heptene	1:10:770	3.5/1.8	83	64
1	*cis*-2-heptene	1:10:250	3.3/1.5	80	65
1	*cis*-2-heptene	1:10:50	3.5/1.5	79	65
1	cyclooctene	1:10:1000	4.7/3.1	84	61
1	cyclohexene	1:10:1000	4.2/1.7	67	57
1	2-methyl-2-heptene	1:10:50	2.0/1.8	81	71
2	1-octene	1:10:1000	2.3/0.9	91	10
2	*trans*-2-heptene	1:10:1000	1.8/1.8	90	10
2	*cis*-2-heptene	1:10:1000	1.5/2.3	90	11
3	1-octene	1:10:1000	2.9/0.5	71	21
3	*trans*-2-heptene	1:10:1000	2.1/2.6	66	22
3	*cis*-2-heptene	1:10:1000	1.8/0.7	63	20

[a] Catalyst/H$_2$O$_2$/substrate. [b] Diol (TN). [c] Epoxide (TN). [d] Percentage of diol ^{16}O^{18}O labeled. [e] Percentage of epoxide ^{18}O labeled.[f] Remaining product is exclusively ^{16}O labeled

We considered different options to rationalize the unexpectedly high level of water incorporation into epoxide products for most of the

olefins studied. The possibility that a radical cation intermediate was initially formed and subsequently trapped by water was discarded, because the involvement of a substrate radical species with a significant lifetime was inconsistent with the high retention of configuration observed for the epoxidation and *cis*-dihydroxylation of *cis*-2-heptene (97% *cis*-epoxide and 95% *cis*-diol, respectively). The possibility that the HO-Fe^V=O oxidant became doubly labeled by rapid, multiple intermolecular exchanges with H$_2$^{18}O prior to its attack of the olefin substrate was also eliminated, because epoxide and *cis*-diol are formed in parallel, and doubly labeled *cis*-diol product was not observed under any conditions tried.

These experiments led us to several mechanistic conclusions. First, the only oxidant in this catalytic system is the HO-Fe^V=O species. Were its Fe^{III}-OOH(OH$_2$) precursor also an oxidant, no label incorporation from water would occur in this pathway, so the extent of label incorporation from water into products would have been observed to decrease with increasing substrate concentration. Furthermore, oxo-hydroxo tautomerism of the HO-Fe^V=O oxidant must be fast relative to substrate oxidation in order to explain the lack of a substrate-concentration dependence on the extent of ^{18}O label incorporation from water. This conclusion suggests that the HO-Fe^V=O oxidant must be fully labeled prior to its reaction with either substrate and that the different extents of label incorporation are a result of specific interactions between substrate and oxidant. Support for this latter notion was found in the competitive oxidation of *cis*-2-heptene and *trans*-2-octene in the presence of H$_2$^{18}O (Scheme 4). Interestingly, *cis*-2-heptene was found to be roughly five times more reactive than *trans*-2-octene, but *cis*-2-heptene oxide incoporated 59% label, while *trans*-2-octene epoxide incorporated only 36%, values similar to those observed in the absence of the other olefin. In other words, the faster reacting substrate incorporated more water than the less reactive substrate. Thus the catalytic behavior of **1** differs from that described for iron and manganese porphyrin catalysts, in which oxo-hydroxo tautomerism competes with substrate oxidation by the high valent species,[2,11] so that the reactivity of a specific substrate is inversely related to the level of water incorporation into products. Clearly, a different mechanistic picture arises from our results.

Scheme 4
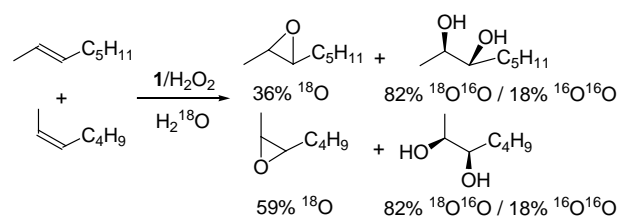
Scheme 5 shows a proposed mechanism for the action of **1** where Fe^{III}OOH(OH$_2$) isomer P$_A$ is more populated than isomer P$_B$.[12] P$_A$ then undergoes rate determining O-O bond cleavage and rapid oxo-hydroxo tautomerism to form O$_A$ and O$_B$ prior to olefin attack. The subsequent reactions of O$_A$ and O$_B$ occur at rates dependent on the structure of the olefin substrate, i.e. k$_A$ ≠ k$_B$. Support for this proposal is obtained by DFT calculations which indicate that isomer P$_A$ is energetically favored over P$_B$ by 2 kcal·mol^{-1}, and the transition state of the heterolytic O-O cleavage of P$_A$ to form O$_A$ is further favored with respect to P$_B$ lysis by 4 kcal·mol^{-1}.[13,14] As demonstrated by the H$_2$^{18}O labeling experiments presented above, *trans*-disubstituted olefins incorporate half as much label from H$_2$^{18}O than *cis*- disubstituted, trisubstituted, and terminal olefins. This difference indicates that *trans* olefins prefer to react with O$_A$ (oxo group not

2

labeled), while the other olefins react preferentially with O_B (oxo group labeled).

The accumulated labeling results for olefin epoxidation reactions catalyzed by **1** present a new twist in the reactivity of the high valent species (O_A and O_B). Despite the large differences in percent label incorporation (33-71%, Table 1), these values in fact translate into only small differences in energy, comparable to those associated with chiral discrimination. Catalyst **1** may give rise to the novel labeling results we observe because the two HO-Fe^V=O oxidants (O_A and O_B), though inequivalent, are quite close to each other in energy (Scheme 5). According to this mechanistic scenario, a C_2-symmetric complex such as **3** should give rise to symmetrically equivalent HO-Fe^V=O species O_A and O_B, and consequently, the level of water incorporation into products must be substrate independent. This is indeed what is observed in Table 1; olefin oxidations catalyzed by **3** afford epoxides incorporating 21 ± 1% of oxygen from water.

Scheme 5
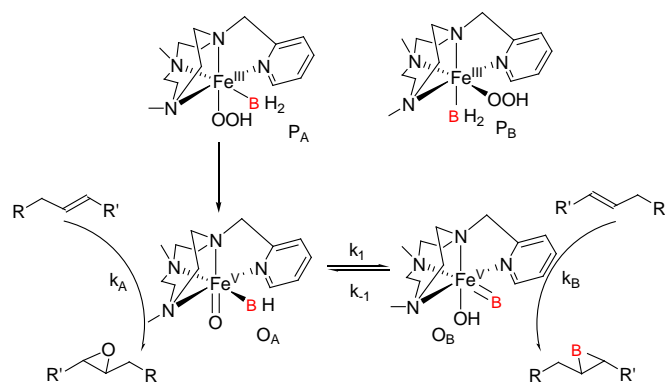
The mechanistic scenario arising from this study may be related to aspects of the catalytic cycle of the α-KG-dependent Cyt-C3 halogenase,[3e] in which two high-spin Fe^{IV}O(X) (X = Cl or Br) intermediates have been characterized by rapid-freeze-quench Mössbauer experiments and found to be directly responsible for the C-H activation event. The relative proportions of these two high-valent isomers remain constant along the reaction coordinate, suggesting that fast interconversion between them precedes substrate oxidation. Indeed, the presence of non-equivalent *cis*-binding sites is a common structural characteristic of a number of nonheme iron oxygenases,[1] and therefore the interplay between two isomerically related high-valent species may be a rather common yet unexpected feature of their oxygen activation chemistry, substantially different from heme systems. The current study serves as a synthetic precedent for this novel mechanistic feature and it calls into question the canonical description of oxygenase action.

[1] a) E. G. Kovaleva; J. D. Lipscomb, *Nat. Chem. Biol.* **2008**, *4*, 186. b) M. Costas, M.; M. P. Mehn; M. P. Jensen, M. P.; L. Que, Jr. *Chem. Rev.* **2004**, *104*, 939. c) M. Abu-Omar; A. Loaiza; N. Hontzeas, *Chem. Rev.* **2005**, *105*, 2227.

[2] a) Ortiz de Montellano, P. R., *Cytochrome P450: Structure, Mechanism and Biochemistry*. 3erd ed.; Kluwer Academic/Plenum Publishers: New York, **2005**. b) B. Meunier; S. P. de Visser; S. Shaik, *Chem. Rev.* **2004**, 104, 3947.

[3] a) J. C. Price; E. W. Barr; T. E. Glass; C. J. Krebs; J. M. Martin Bollinger, Jr. *J. Am. Chem . Soc.* **2003**, *125*, 13008. b) P. Riggs-Gelasco; J. C. Price; R. B. Guyer; J. H. Brehm; E. W. Barr; J. M. Bollinger Jr.; C. Krebs *J. Am. Chem . Soc.* **2004**, *126*, 8108. c) S. S. Sinnecker; E. W. Barr, S. Ye; J. M., Jr. Bollinger; F. Neese, ; C. Krebs *J. Am. Chem. Soc.* **2007**, *129*, 6168. d) C. Krebs; D. Galonić Fujimori; C. T. Walsh; J. M. Bollinger, *Acc. Chem. Res.* **2007**, *40*; 484. e) D. P. Galonić; E. W. Barr; C. T. Walsh; J. M. Bollinger; C. Krebs, C. *Nat. Chem. Biol.* **2007**, *3*, 113. f) M. D. Wolfe; D. J. Altier; A. Stubna; C. V. Popescu; E. Münck; J. D. Lipscomb *Biochemistry* **2002**, *41*, 9611. g) M. D. Wolfe; J. D. Lipscomb *J. Biol. Chem.* **2003**, *278*, 829.

[4] a) J.-U Rohde; J.-H In; M.-H. Lim; W. W. Brennessel; M. R. Bukowski; A. Stubna; E. Münck; W. Nam; L. Que, Jr. *Science* **2003**, *229*, 1037. b) E. J. Klinker; J. Kaizer; W. W. Brennessel; N. L. Woodrum; C. J. Cramer; L. Que Jr., L. *Angew. Chem.* **2005**, *117*, 3756. *Angew. Chem. Int. Ed.* **2005**, *44*, 3690. c) J. Kaizer; E. Klinker; N. Y. Oh; J.-U. Rohde; W. J. Song; A. Stubna; J. Kim; E. Munck; W. Nam; L. Que, Jr. *J. Am. Chem. Soc.* **2004**, *126*, 472. d) K. Chen; L. Que, Jr. *J. Am. Chem. Soc.* **2001**, *123*, 6327. e) F. Tiago de Oliveira; A. Chanda; D. Banerjee; X. Shan; S. Mondal; L. Que, Jr.; E. L. Bominaar; E. Münck; T. J. Collins, *Science* **2007**, *215*, 835. f) M. Martinho; F. Banse; J.-F. Bartoli; T. A. Mattioli; P. Battioni; O. Horner; S. Bourcier; J.-J Girerd, *Inorg. Chem.* **2005**, *44*, 9592. g) J. Bautz; M. R. Bukowski; M. Kerscher; A. Stubna; P. Comba; A. Lienke; E. Münck; L. Que Jr. *Angew. Chem.* **2006**, *118*, 5810, *Angew. Chem. Int Ed.* **2006**, 45, 5681. h) M. R. Bukowski, P. Comba, A. Lienke, C. Limberg, C. Lopez de Laorden, R. Mas-Ballesté, M. Merz, L. Que Jr. *Angew. Chem.* **2006**, *118*, 3524. *Angew. Chem. Int. Ed.* **2006**, *45*, 3446. i) C. A. Graperhaus, B. Mienert, E. Bill, T. Weyhermüller, K. Wieghardt *Inorg. Chem.* **2000**, *39*, 5306. j) T. A. van den Berg, J. W. de Boer, W. R. Browne, G. Roelfes and B. L. Feringa, *Chem. Commun.,* **2004**, *22*, 2550.

[5] A. Company; L. Gómez; M. Güell; X. Ribas; J. M. Luis; L. Que, Jr.; M. Costas *J. Am. Chem. Soc.* **2007**, *129*, 15766.

[6] A. Company; L. Gómez; X. Fontrodona; X. Ribas; M. Costas *Chem. Eur. J.* **2008***, 14*, 5727.

[7] For selected examples of Fe-TACN complexes in oxidation catalysis see a) V. B. Romakh; B. Therrien; G. Labat; H. Soekli-Evans; G. B. Shul'pin; G. Süss-Fink *Inorg. Chim. Acta,* **2006**, *359*, 3297. b) V. B. Romakh; B. Therrien; G. Süss-Fink; G. B. Shul'pin, *Inorg. Chem.* **2007**, *46*, 3166.

[8] a) K. Chen; M. Costas; J. Kim; A. K. Tipton; L. Que, Jr. *J. Am. Chem. Soc.* **2002**, *124*, 3026. b) K. Chen; L. Que, Jr. *Chem. Commun.* **1999**, 1375.

[9] a) D. Quinonero; K. Morokuma; D. G. Musaev; R. Mas-Balleste; L. Que, Jr. *J. Am. Chem. Soc.* **2005**, *127*, 6548. b) A. Bassan; M. R. A. Blomberg; P. E. M. Siegbahn; L. Que Jr. *Chem. Eur. J.* **2005**, *11*, 692.

[10] A. Bassan, M. R. A. Blomberg, P. E. M. Siegbahn, L. Que. Jr. *Angew. Chem.* **2005***, 117*, 2999*, Angew. Chem. Int. Ed.* **2005**, *44*, 2939.

[11] a) J. Bernadou; B. Meunier *Chem. Commun.* **1998**, 2167. b) M. S. Seo; T. Kamachi; T. Kouno; K. Murata; M. J. Park; K. Yoshizawa; W. Nam *Angew. Chem.* **2007**, *119*,2341*, Angew. Chem. Int. Ed.* **2007**, *46*, 2291.

[12] Notice that if peroxide binding in, and/or O-O breakage in species P_A and P_B was identical, all epoxides would be 50% water-labeled.

[13] DFT geometries were optimized at the B3LYP level in junction of the LANL2DZ basis set with associated ECP for Fe as implemented in the Gaussian 03 program. The energies were further refined by single-point calculations using the SDD basis set with associated ECP for Fe and 6-311G(d,p) basis sets on the other atoms. Final free energies given in this work include energies computed at the B3LYP/6-311G(d,p)&SDD //B3LYP/LANL2DZ level of theory together with zero-point energies, thermal corrections and entropy calculated at the B3LYP/LANL2DZ level.

[14] Analogous differences in energy between tautomeric ferric-hydroperoxide species have been described for [Fe(TPA)(OOH)(H$_2$O)]$^{2+}$, A. Bassan, M. R. A.; Blomberg, P. E. M. Siegbahn, L. Que, Jr. *J. Am. Chem. Soc.* **2002**, *124*, 11056

Entry for the Table of Contents
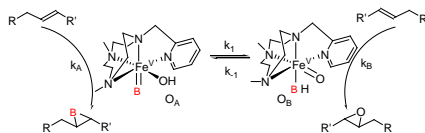
Fast equilibrium between two high valent HO-Fe^V=O isomeric species with different reactivity leads to substrate dependent water incorporation into products in epoxidation reactions with H$_2$O$_2$ by a bioinspired non-heme iron catalyst.

Olefin-Dependent Discrimination Between Two Nonheme OH-Fe^V=O Tautomeric Species in Catalytic H$_2$O$_2$ Epoxidations

Anna Company,[a] Yan Feng,[b] Mireia Güell,[c] Xavi Ribas,[a] Josep M. Luis,[c]

Lawrence Que, Jr.[b],* and Miquel Costas[a],*

[a]*Departament de Química, Universitat de Girona, Campus de Montilivi, E-17071 Girona, Spain.* [b]*Department of Chemistry and Center for Metals in Biocatalysis, University of Minnesota, Minneapolis, Minnesota 55455.* [c]*Institute of Computational Chemistry, Universitat de Girona, Campus de Montilivi, E-17071 Girona, Spain.*

Contents

1) Experimental section

Materials and synthesis

Reagents and solvents used were of commercially available reagent quality unless otherwise stated. $H_2^{18}O_2$ (90% ^{18}O-enriched, 2% solution in H_2O) and $H_2^{18}O$ (95% ^{18}O-enriched) were received from ICON Isotopes. Solvents were purchased from SDS. CH_3CN was distilled over CaH_2 under nitrogen.

$[Fe(CF_3SO_3)_2(^{Me2}PyTACN)]$ (**1**),[1] $[Fe(CF_3SO_3)_2(TPA)]$ (**2**)[2] and $[Fe(CF_3SO_3)_2(BPMEN)]$ (**3**)[2] were prepared following experimental procedures previously reported.

Instrumentation

Product analyses were performed on a Shimadzu GC-2010 gas chromatograph (Cyclodex-B column, 30 m) or on a Perkin-Elmer Autosystem XL gas chromatograph (AT-1701 column, 30 m) and a flame ionization detector. GC-MS spectral analyses were performed on a ThermoQuest Trace GC 2000 Series chromatograph interfaced with a Finnigan ThermoQuest Trace MS mass spectrometer or on a HP6890 GC (HP-5 column, 30 m) with an Agilent 5973 mass detector using a 4% NH_3/CH_4 mix as the ionization gas for chemical ionization analyses. The products were identified by comparison of their GC retention times and GC/MS with those of authentic compounds.

Reaction conditions for catalysis

In a typical reaction, 0.36 mL of a 70 mM (25 μmols) H_2O_2 solution (diluted from a 35% H_2O_2 aqueous solution) together with 45 μL of H_2O (2500 μmols) in CH_3CN was delivered by syringe pump over 30 min at 25 ºC under N_2 to a vigorously stirred CH_3CN solution (2.14 mL) containing the iron catalyst (2.5 μmols) and the substrate (2500 μmols). The final concentrations of the reagents were 1 mM iron catalyst (**1**, **2** or **3**), 10 mM H_2O_2, 1 M H_2O and 1 M substrate. After syringe pump addition, the resulting solution was stirred for another 10 min. Addition of 1 mL acetic anhydride together with 0.1 mL 1-methylimidazole afforded the esterification of the *cis*-diol products. After stirring for 15 min at room temperature, ice was added and the mixture was stirred for about 30 min. Biphenyl or naphthalene (internal standard) was added at this point and the mixture was extracted with 2 mL $CHCl_3$. The organic layer was washed with 2 mL H_2SO_4 1 M, 2 mL sat. $NaHCO_3$ and 2 mL H_2O, dried with $MgSO_4$ and subjected to GC analysis. The organic products were identified by comparison with authentic compounds.

Isotope labeling studies

Reaction catalytic conditions using $H_2^{18}O$: In a typical reaction, 0.29 mL of a 70 mM (20 μmols) H_2O_2 solution (diluted from a 35% H_2O_2 aqueous solution) together with 40 μL of $H_2^{18}O$ (2000 μmols) in CH_3CN was delivered by syringe pump over 30 min at 25 ºC under N_2 to a vigorously stirred CH_3CN solution (1.71 mL) containing the iron catalyst (2.0 μmols) and the substrate

(2000 µmols). The final concentrations of reagents were 1 mM iron catalyst (**1**, **2** or **3**), 10 mM H_2O_2, 1 M $H_2^{18}O$ and 1 M substrate. After syringe pump addition, the resulting solution was stirred for another 10 min. The reaction solutions were treated with 0.1 mL 1-methylimidazole and 1 mL acetic anhydride to esterify the diol products following the experimental procedure described above.

Several experiments at different substrate concentration were run for *cis*-2-heptene and catalyst **1**. In these reactions, the experimental procedure was the same as described above but changing the amount of substrate to achieve the desired final concentration.

Several experiments at different $H_2^{18}O$ concentrations were run for cyclooctene and catalyst **1**. In these reactions, the experimental procedure was the same as described above but using the appropriate amount of labeled water.

Reaction catalytic conditions using $H_2^{18}O_2$: 0.29 mL of a 70 mM (20 µmols) $H_2^{18}O_2$ solution (diluted from a 2% $H_2^{18}O_2$ aqueous solution) in CH_3CN was delivered by syringe pump over 30 min at 25 ºC under N_2 to a vigorously stirred CH_3CN solution (1.71 mL) containing the iron catalyst (2.0 µmols) and cyclooctene (2000 µmols). The final concentrations of reagents were 1 mM iron catalyst (**1**), 10 mM $H_2^{18}O_2$, 1 M H_2O and 1 M cyclooctene. After syringe pump addition, the resulting solution was stirred for another 10 min. The reaction solutions were treated with 0.1 mL 1-methylimidazole and 1 mL acetic anhydride to esterify the diol products following the experimental procedure described above.

2) Catalytic results

% of ^{18}O-labeled cis-diol and epoxide vs [$H_2^{18}O$]

Table S1. Percentage of singly ^{18}O-labeled *cis*-diol (% $^{18}O^{16}O$-diol) and ^{18}O-labeled epoxide (% ^{18}O-epoxide) in the oxidation of cyclooctene by complex **1** at different $H_2^{18}O$ concentrations.

equiv H_2O_2	equiv $H_2^{18}O$	[$H_2^{18}O$] (M)	% $^{18}O^{16}O$-diol[a]	% ^{18}O-epoxide[b]
10	50	0.05	39	16
10	100	0.10	54	27
10	250	0.25	69	41
10	500	0.50	74	55
10	1000	1.00	85	62
10	1500	1.50	86	60

Reaction catalytic conditions: 0.29 mL of a 70 mM (20 µmols) H_2O_2 solution (diluted from a 35 % H_2O_2 solution in CH_3CN) together with the appropriate amount of $H_2^{18}O$ (from 100 to 3000 µmols) was delivered by syringe pump over 30 min at 25 ºC to a CH_3CN solution (1.71 mL) containing the iron catalyst (2.0 µmols) and cyclooctene (2000 µmols) under N_2.
[a] Fraction of singly ^{18}O-labeled *cis*-diol. [b] Fraction of ^{18}O-labeled epoxide.

Figure S1. Fraction of singly ^{18}O-labeled *cis*-diol (a) and fraction of ^{18}O-labeled epoxide (b) obtained in cyclooctene oxidation catalysed by **1**/H_2O_2 as a function of the concentration of $H_2^{18}O$ ([$H_2^{18}O$]). Insets: Double-reciprocal plots.
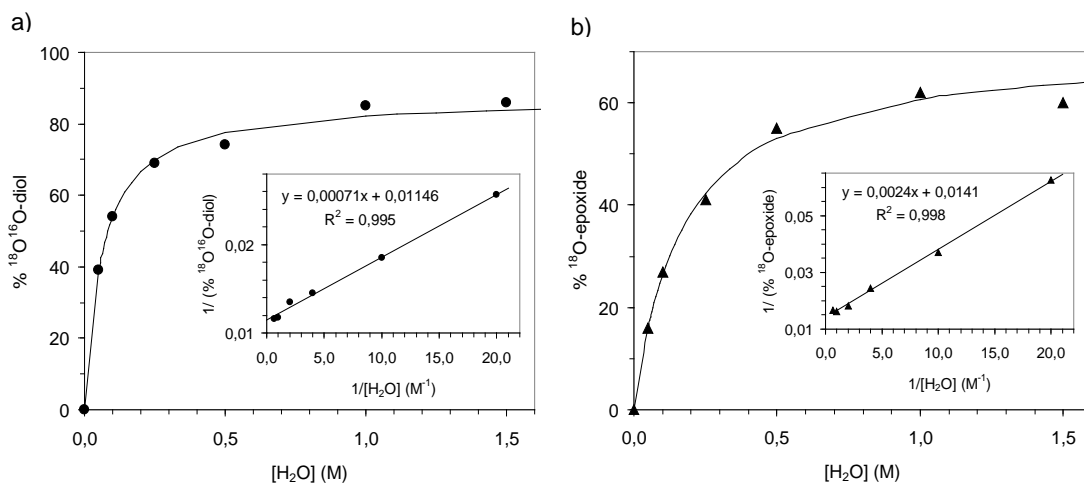
Competition experiment between cis-2-heptene and trans-2-octene
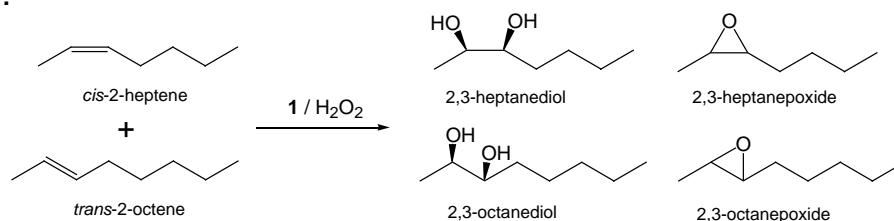
Scheme 1.

Table S2. Turnover numbers and labeling results obtained in the competitive oxidation catalyzed by **1** of *cis*-2-heptene and *trans*-2-octene (Scheme 1).

2,3-heptanediol[a] (TN)	2,3-heptanepoxide[b] (TN)	2,3-octanediol[c] (TN)	2,3-octanepoxide[d] (TN)
2.5	1.2	1.6	0.9
↓	↓	↓	↓
% $^{18}O^{16}O$-diol[e]	% ^{18}O-epoxide[f]	% $^{18}O^{16}O$-diol[e]	% ^{18}O-epoxide[f]
82	59	82	36

Reaction catalytic conditions: 0.29 mL of a 70 mM (20 μmols) H_2O_2 solution (diluted from a 35 % H_2O_2 solution in CH_3CN) together with 40 μL of $H_2^{18}O$ (2 mmols) was delivered by syringe pump over 30 min at 25 ºC to a CH_3CN solution (1.71 mL) containing the iron catalyst (2.0 μmols), *trans*-2-octene (150 μmols) and *cis*-2-heptene (50 μmols) under N_2. Products obtained in the oxidation of *cis*-2-heptene: 2,3-heptanediol and 2,3-heptanepoxide. Products obtained in the oxidation of *trans*-2-octene: 2,3-octanediol and 2,3-octanepoxide.
[a] TN = mols 2,3-heptanediol/mols catalyst. [b] TN = mols 2,3-heptanepoxide/mols catalyst. [c] TN = mols 2,3-octanediol/mols catalyst. [d] TN = mols 2,3-octanepoxide/mols catalyst. [e] Percentage of singly ^{18}O-labeled *cis*-diol. [f] Percentage of ^{18}O-labeled epoxide.

3) Theoretical calculations

Figures S2-S7 show the structures of P$_A$, P$_B$, the stationary points located on the PES for the reaction mechanism studied at the B3LYP level of theory with the LANL2DZ basis set with associated ECP for Fe.

Figure S2. Structure of the P$_A$ structure at the B3LYP level of theory with the LANL2DZ basis set with associated ECP for Fe.
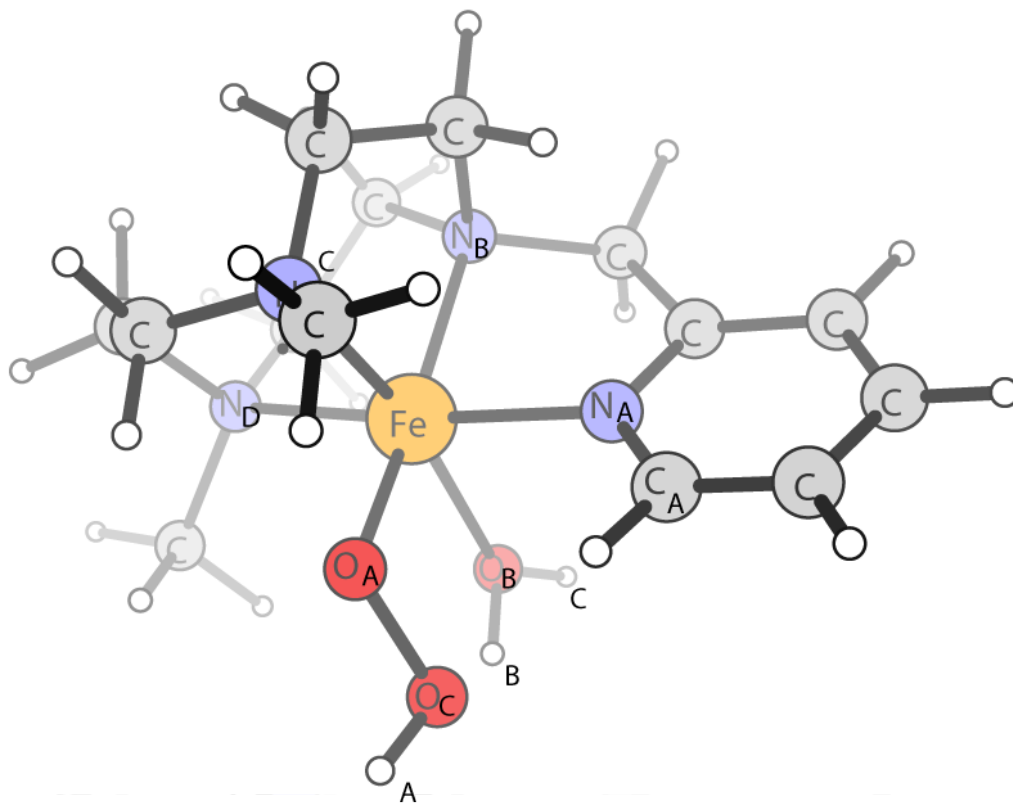
Figure S3. Structure of the P$_B$ structure at the B3LYP level of theory with the LANL2DZ basis set with associated ECP for Fe.
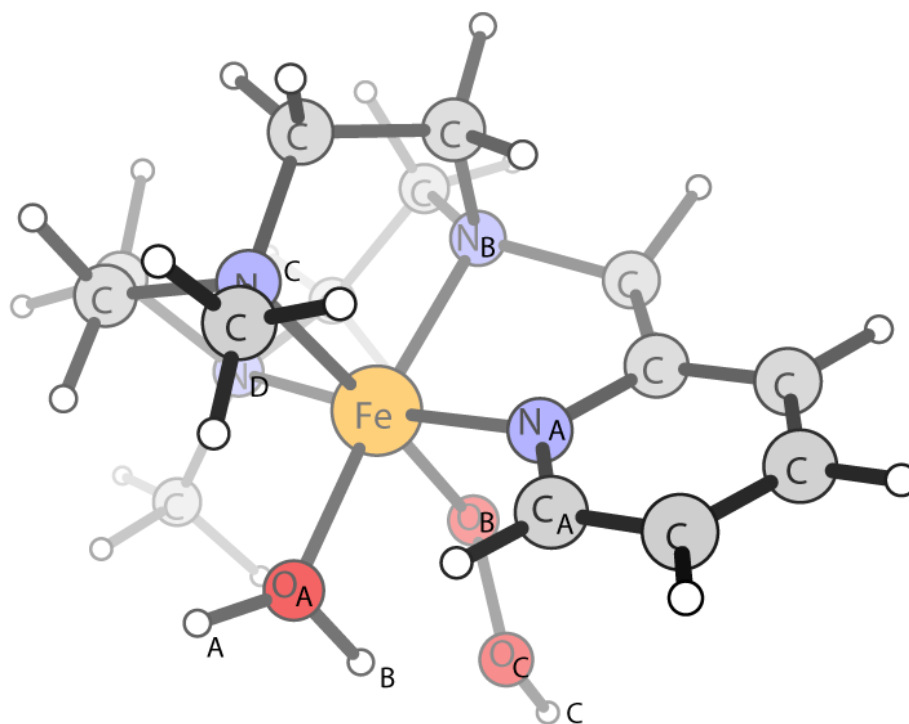
Figure S4. Structure of the O_A structure at the B3LYP level of theory with the LANL2DZ basis set with associated ECP for Fe.
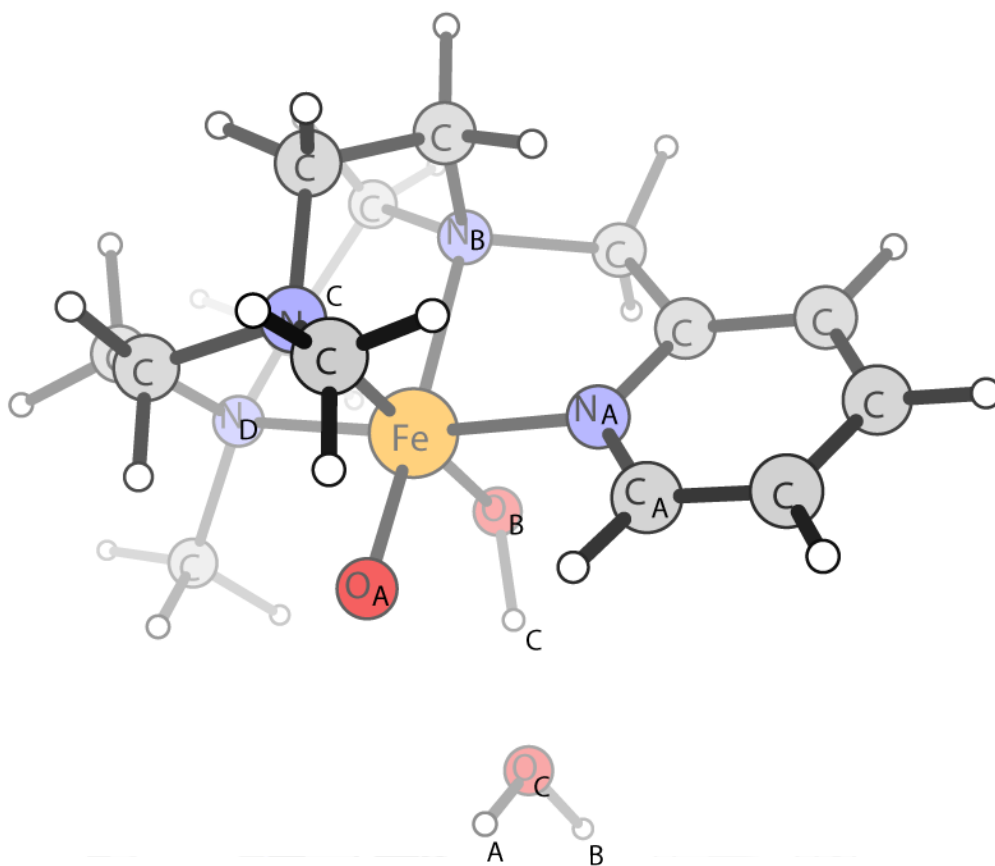
Figure S5. Structure of the O_B structure at the B3LYP level of theory with the LANL2DZ basis set with associated ECP for Fe.
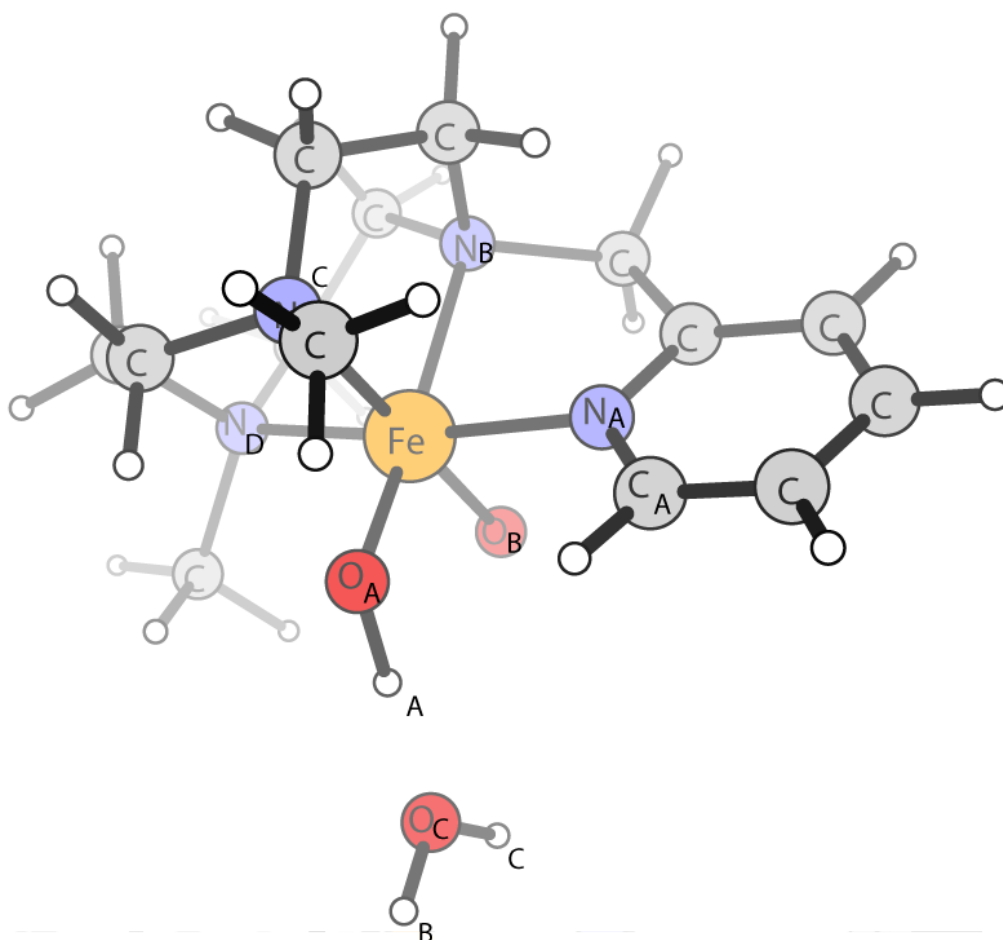
Figure S6. Structure of the structure of the transition state connecting P_A and O_A at the B3LYP level of theory with the LANL2DZ basis set with associated ECP for Fe.
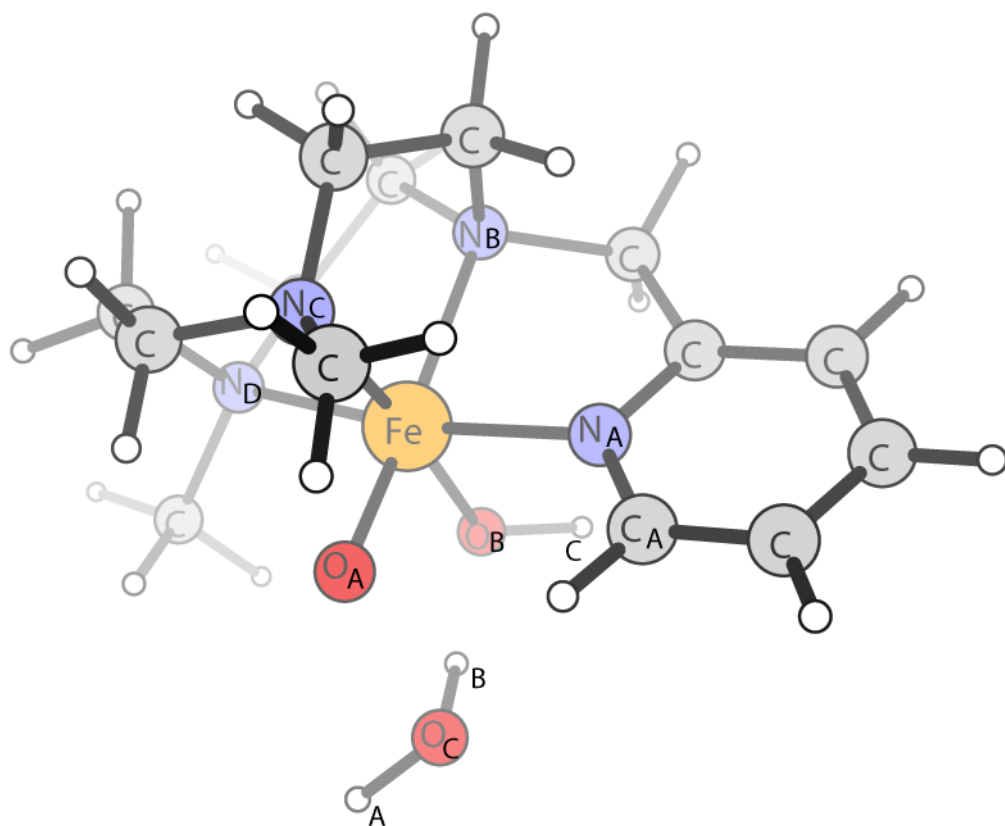
Figure S7. Structure of the structure of the transition state connecting P$_B$ and O$_B$ at the B3LYP level of theory with the LANL2DZ basis set with associated ECP for Fe.
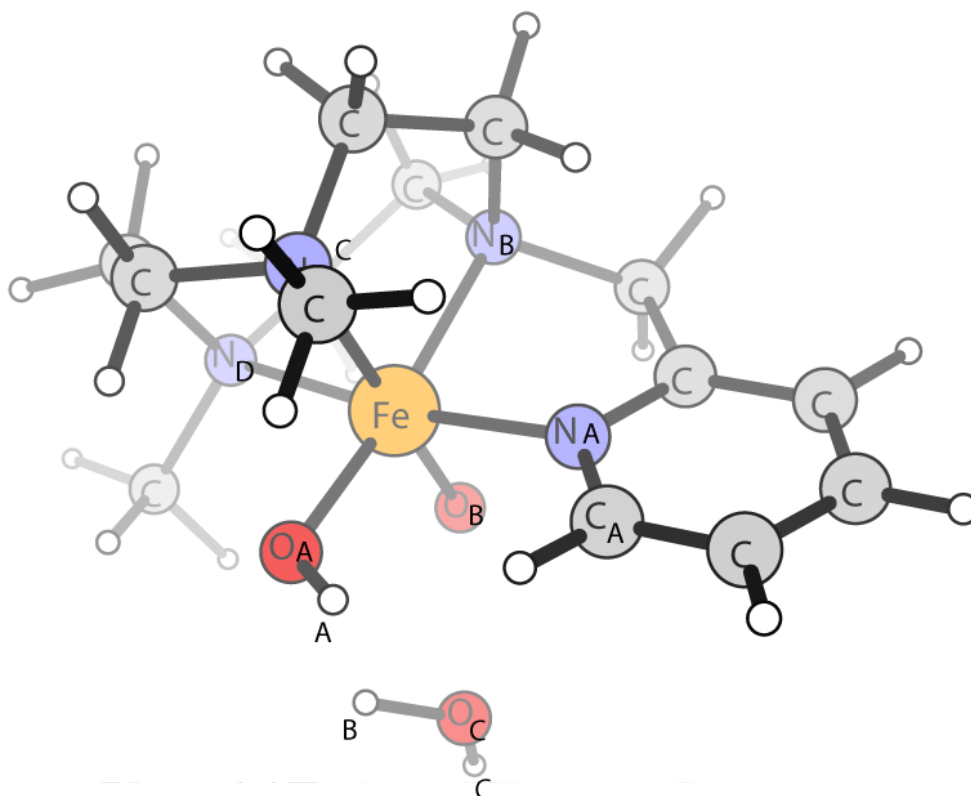
Table S3. Selected structural parameters (in Å) for P$_A$, P$_B$, O$_A$, O$_B$ and the transition states for P$_A$-O$_A$ and P$_B$-O$_B$ arising from the DFT analyses

	Fe-N$_A$	Fe-N$_B$	Fe-N$_C$	Fe-N$_D$	Fe-O$_A$	Fe-O$_B$	O$_A$-O$_C$	O$_B$-O$_C$	O$_C$-H$_B$
P$_A$	2.003	2.033	2.042	2.043	1.834	2.052	1.506	2.487	1.628
TS(P$_A$-O$_A$)	1.999	2.066	2.086	2.040	1.675	1.927	2.004	2.437	1.084
O$_A$	1.999	2.076	2.129	2.048	1.754	1.679	3.164	2.528	1.042
P$_B$	1.997	1.988	2.072	2.057	2.025	1.850	2.497	1.504	1.677
TS(P$_B$-O$_B$)	2.014	2.032	2.131	2.061	1.848	1.708	2.681	2.124	0.992
O$_B$	2.007	2.065	2.140	2.042	1.754	1.679	2.530	3.223	0.976

Table S4. Calculated spin densities for P_A, P_B, O_A, O_B and the transition states for P_A-O_A and P_B-O_B

	Fe	N_A	N_B	N_C	N_D	O_A	O_B	O_C
P_A	0.941	-0.003	-0.019	-0.033	-0.019	0.142	-0.007	0.005
TS(P_A-O_A)	1.521	-0.012	-0.022	-0.043	-0.030	0.049	-0.014	-0.466
O_A	1.770	-0.005	-0.033	-0.020	-0.037	0.980	0.341	0.005
P_B	0.959	-0.020	-0.033	-0.023	-0.021	-0.006	0.128	0.010
TS(P_B-O_B)	1.755	-0.033	-0.042	-0.012	-0.059	0.049	-0.369	-0.295
O_B	1.711	0.003	-0.021	-0.040	-0.025	0.360	1.012	0.005

Tables S5-S10 show the optimized cartesian xyz coordinates of the stationary points located on the PES for the reaction mechanism studied at the B3LYP level of theory with the LANL2DZ basis set with associated ECP for Fe.

Table S5. Optimized cartesian xyz coordinates of the P$_A$ structure at the B3LYP level of theory with the LANL2DZ basis set with associated ECP for Fe.

atom	X	Y	Z
H	0.668885	-1.827944	3.004413
H	2.950559	0.065001	2.616986
H	1.949469	-2.027867	1.821896
C	0.947471	-1.618466	1.966187
H	3.314784	-1.216518	0.523343
H	0.086573	-3.356104	0.975801
C	2.419467	0.385989	1.710899
H	1.920917	-2.771383	-0.374269
H	4.080658	0.348987	0.322521
C	0.220538	0.593855	2.834048
C	3.112041	-0.144522	0.453594
N	0.983663	-0.111628	1.735718
C	-0.054353	-2.268208	1.015385
H	2.383233	1.478564	1.703071
H	-1.074515	-2.075448	1.354492
C	1.324740	-2.206186	-1.095494
H	1.028231	-2.913742	-1.878072
H	3.150079	-1.409300	-1.973707
N	0.093855	-1.668808	-0.373988
N	2.226877	0.123844	-0.757146
C	2.143087	-1.057935	-1.710351
H	-1.538136	-2.912490	-1.055292
C	2.763424	1.326673	-1.501946
C	-1.199739	-1.870901	-1.129564
H	1.667883	-0.687124	-2.621884
Fe	0.293983	0.340002	-0.132686
H	-1.020013	-1.668910	-2.192544
C	-2.226106	-0.913246	-0.545421
N	-1.691013	0.183426	0.083005
H	-4.018762	-1.977177	-1.115631
C	-3.610608	-1.098750	-0.624994
C	-2.507349	1.123372	0.630362
H	-2.027200	1.980689	1.084864
C	-4.463960	-0.130139	-0.055598
C	-3.903547	0.993057	0.580344
H	-5.541443	-0.253478	-0.106831
H	-4.529773	1.758154	1.026034
H	2.105313	1.569785	-2.335683
H	3.766061	1.103365	-1.888139
H	2.818702	2.177381	-0.820378
H	-0.797853	0.201335	2.884177
H	0.189211	1.663627	2.623175
H	0.714341	0.425828	3.799428
O	-0.165853	0.953094	-2.036384
O	0.446865	2.111644	0.315018
H	-0.253659	1.946303	-1.877816
H	-0.885869	0.617868	-2.603449
O	-0.272899	3.015185	-0.650593
H	0.099558	3.905775	-0.448825

Table S6. Optimized cartesian xyz coordinates of the P_B structure at the B3LYP level of theory with the LANL2DZ basis set with associated ECP for Fe.

atom	X	Y	Z
H	-0.736380	-3.493619	-0.320410
H	-3.006124	-2.061046	-1.661717
H	-2.040008	-2.642310	0.485575
C	-1.026370	-2.523573	0.097422
H	-3.362688	-1.089627	0.587563
H	-0.247769	-2.708091	2.122373
C	-2.463026	-1.142833	-1.399033
H	-2.001470	-1.236670	2.431289
H	-4.121657	-0.016076	-0.571929
C	-0.271278	-1.969844	-2.208210
C	-3.154385	-0.412682	-0.244704
N	-1.032605	-1.467361	-1.006021
C	-0.055259	-2.128295	1.210846
H	-2.431011	-0.516933	-2.297150
H	0.972517	-2.329587	0.902979
C	-1.396077	-0.328337	2.362237
H	-1.091358	-0.072531	3.382952
H	-3.219050	0.848719	2.175680
N	-0.170786	-0.638506	1.512013
N	-2.260163	0.717957	0.237739
C	-2.204805	0.830676	1.754035
H	1.445994	-0.802228	2.939151
C	-2.762821	2.026134	-0.330225
C	1.141919	-0.158751	2.104024
H	-1.727387	1.788455	1.974879
Fe	-0.299773	0.309154	-0.230991
H	0.996072	0.859316	2.476976
C	2.174257	-0.159394	0.990454
N	1.662484	-0.059215	-0.279408
H	3.941048	-0.320237	2.221744
C	3.553385	-0.236092	1.211224
C	2.500671	-0.021319	-1.348845
H	2.043701	0.084721	-2.324720
C	4.426679	-0.198980	0.105675
C	3.891293	-0.094046	-1.191999
H	5.500777	-0.252470	0.255204
H	4.534028	-0.061867	-2.064918
H	-2.041701	2.815738	-0.120139
H	-3.729096	2.282752	0.122038
H	-2.905575	1.933850	-1.410586
H	0.727656	-2.288855	-1.904104
H	-0.177848	-1.172582	-2.948382
H	-0.792276	-2.823296	-2.660880
O	0.096314	1.951299	0.522182
O	-0.185110	1.242380	-2.024288
H	0.326366	2.076322	-1.795278
H	-0.844949	1.370694	-2.729013
O	0.989415	2.732844	-0.401917
H	1.059731	3.611167	0.041117

Table S7. Optimized cartesian xyz coordinates of the O$_A$ structure at the B3LYP level of theory with the LANL2DZ basis set with associated ECP for Fe.

atom	X	Y	Z
H	-0.743187	-3.468690	-0.927281
H	-2.942072	-1.790427	-2.068562
H	-2.027678	-2.740484	0.020423
C	-1.012194	-2.579251	-0.346891
H	-3.365916	-1.228794	0.309908
H	-0.214177	-3.139073	1.598393
C	-2.401936	-0.940504	-1.629493
H	-1.990994	-1.746489	2.145842
H	-4.072679	0.046347	-0.670353
C	-0.191207	-1.630239	-2.496413
C	-3.124857	-0.422496	-0.386975
N	-0.992889	-1.353406	-1.247585
C	-0.032868	-2.395607	0.811108
H	-2.320466	-0.158572	-2.389625
H	0.992116	-2.532373	0.459767
C	-1.394178	-0.834628	2.241780
H	-1.111184	-0.753473	3.297248
H	-3.242498	0.320545	2.221223
N	-0.152511	-0.992996	1.375939
N	-2.247163	0.598589	0.328796
C	-2.215310	0.406471	1.841952
H	1.462076	-1.396847	2.758904
C	-2.736519	1.996157	0.005914
C	1.150241	-0.620806	2.048799
H	-1.764786	1.308782	2.255842
Fe	-0.282356	0.356238	-0.196965
H	1.000964	0.319202	2.588359
C	2.182284	-0.415566	0.955116
N	1.674421	-0.045630	-0.265405
H	3.956986	-0.849330	2.103197
C	3.562983	-0.548538	1.137478
C	2.498776	0.227323	-1.311325
H	2.032018	0.552181	-2.233713
C	4.429213	-0.279148	0.058094
C	3.889583	0.112874	-1.181804
H	5.503690	-0.371164	0.184614
H	4.527395	0.333486	-2.030751
H	-2.072230	2.732659	0.457828
H	-3.751408	2.124990	0.402672
H	-2.745030	2.136702	-1.077219
H	0.804370	-1.989577	-2.226783
H	-0.104451	-0.712701	-3.081340
H	-0.692451	-2.398185	-3.099460
O	0.102331	1.694175	0.894712
O	-0.324903	1.238822	-1.605135
H	0.322785	2.603318	0.436849
O	0.584838	3.922104	-0.197721
H	0.898741	4.712456	0.280775
H	0.506115	4.080376	-1.156789

Table S8. Optimized cartesian xyz coordinates of the O_B structure at the B3LYP level of theory with the LANL2DZ basis set with associated ECP for Fe.

atom	X	Y	Z
H	0.540417	-2.550997	2.526865
H	2.864463	-0.634808	2.640486
H	1.851109	-2.494442	1.365575
C	0.852876	-2.104160	1.576499
H	3.266253	-1.415685	0.325087
H	-0.010679	-3.542425	0.185539
C	2.347040	-0.114345	1.822552
H	1.855984	-2.728233	-0.950892
H	4.044265	0.149557	0.503602
C	0.129665	-0.135008	2.910093
C	3.071914	-0.353795	0.496182
N	0.915314	-0.593208	1.707571
C	-0.133159	-2.490654	0.475646
H	2.311126	0.951449	2.059646
H	-1.158790	-2.361465	0.827383
C	1.299920	-1.990233	-1.535553
H	1.005098	-2.482078	-2.469196
H	3.192093	-1.086334	-2.122314
N	0.061562	-1.595912	-0.738411
N	2.236752	0.184853	-0.662053
C	2.176863	-0.766850	-1.851819
H	-1.566369	-2.595610	-1.750919
C	2.794278	1.520766	-1.111726
C	-1.219555	-1.574509	-1.549671
H	1.763529	-0.198227	-2.687553
Fe	0.280108	0.356763	-0.102194
H	-1.015753	-1.079274	-2.504667
C	-2.240614	-0.779870	-0.758595
N	-1.704412	0.140115	0.104830
H	-4.043216	-1.659508	-1.557172
C	-3.626725	-0.923407	-0.876717
C	-2.502952	0.947805	0.849525
H	-2.009995	1.669632	1.488823
C	-4.468908	-0.095621	-0.105969
C	-3.899400	0.848046	0.769521
H	-5.547625	-0.187068	-0.188691
H	-4.518715	1.500788	1.375009
H	2.134144	1.961187	-1.860442
H	3.792639	1.371130	-1.541308
H	2.860801	2.190486	-0.252458
H	-0.885185	-0.538100	2.864513
H	0.092274	0.955038	2.915973
H	0.608344	-0.490564	3.831914
O	-0.042980	1.014738	-1.612948
O	0.416443	1.873650	0.767796
H	0.257313	2.754484	0.235161
H	-0.327613	4.088484	-1.396264
O	0.022973	4.034174	-0.487790
H	0.137820	4.916319	-0.086491

Table S9. Optimized cartesian xyz coordinates of the transition state connecting O_A and P_A at the B3LYP level of theory with the LANL2DZ basis set with associated ECP for Fe.

atom	X	Y	Z
H	0.723700	-2.488444	2.520202
H	2.961307	-0.518016	2.586954
H	1.998582	-2.374638	1.319645
C	0.989752	-2.033317	1.560236
H	3.347950	-1.240012	0.253201
H	0.153090	-3.501878	0.190482
C	2.417619	0.005869	1.789364
H	1.973573	-2.586835	-0.980753
H	4.067998	0.350538	0.433075
C	0.210383	-0.102321	2.921021
C	3.115250	-0.188611	0.440663
N	0.993403	-0.516065	1.696208
C	-0.005523	-2.456512	0.485791
H	2.360423	1.065337	2.052733
H	-1.027290	-2.368003	0.861325
C	1.365873	-1.878662	-1.550731
H	1.078570	-2.385897	-2.478701
H	3.177867	-0.865550	-2.207584
N	0.128569	-1.547536	-0.724697
N	2.225242	0.331261	-0.682684
C	2.161474	-0.605086	-1.882810
H	-1.489428	-2.632588	-1.657417
C	2.726463	1.684270	-1.139146
C	-1.170091	-1.594590	-1.500202
H	1.675493	-0.041254	-2.680763
Fe	0.289580	0.396275	-0.043122
H	-1.004307	-1.152509	-2.488983
C	-2.205190	-0.811122	-0.708968
N	-1.684692	0.139950	0.134502
H	-3.988475	-1.759869	-1.473848
C	-3.587415	-0.997623	-0.812814
C	-2.504921	0.943888	0.862507
H	-2.030100	1.706692	1.466927
C	-4.448154	-0.178536	-0.051281
C	-3.899227	0.803295	0.793939
H	-5.524307	-0.304279	-0.121518
H	-4.532051	1.457146	1.383982
H	2.044751	2.085906	-1.888170
H	3.725829	1.572955	-1.578041
H	2.780606	2.357186	-0.280773
H	-0.796367	-0.524228	2.875087
H	0.147303	0.986336	2.961505
H	0.709955	-0.472584	3.825073
O	-0.106239	1.279314	-1.709107
O	0.392055	1.862927	0.759517
H	-0.273699	2.557645	-1.145810
H	-0.944214	1.067725	-2.171237
O	-0.490497	3.271924	-0.359831
H	0.156220	3.993748	-0.188793

Table S10. Optimized cartesian xyz coordinates of the transition state connecting O_B and P_B at the B3LYP level of theory with the LANL2DZ basis set with associated ECP for Fe.

atom	X	Y	Z
H	0.827391	-3.289074	1.310725
H	3.000092	-1.430943	2.227769
H	2.078628	-2.652618	0.258647
C	1.067715	-2.467731	0.626866
H	3.402064	-1.171931	-0.209650
H	0.228675	-3.258443	-1.221839
C	2.440853	-0.656298	1.685498
H	1.997667	-1.938429	-1.947800
H	4.088598	0.226425	0.601611
C	0.258035	-1.288549	2.655745
C	3.147707	-0.288698	0.382278
N	1.038157	-1.143063	1.372304
C	0.060645	-2.432489	-0.518786
H	2.338477	0.221935	2.326099
H	-0.956356	-2.526832	-0.132291
C	1.395128	-1.049418	-2.152121
H	1.094069	-1.105640	-3.203984
H	3.237191	0.102708	-2.300461
N	0.160908	-1.103945	-1.255286
N	2.252864	0.622982	-0.449454
C	2.215129	0.237060	-1.921726
H	-1.462269	-1.713194	-2.544539
C	2.715949	2.054279	-0.303425
C	-1.155712	-0.837390	-1.959236
H	1.766231	1.078168	-2.454618
Fe	0.281906	0.397077	0.109332
H	-1.021006	0.009213	-2.639864
C	-2.187222	-0.487065	-0.900967
N	-1.688045	0.013029	0.278198
H	-3.942366	-1.029701	-2.031975
C	-3.564755	-0.626946	-1.097239
C	-2.538704	0.391340	1.268249
H	-2.112575	0.783381	2.183861
C	-4.450410	-0.231424	-0.075137
C	-3.927874	0.279802	1.127144
H	-5.523257	-0.323020	-0.214247
H	-4.577140	0.592395	1.937528
H	2.066310	2.705757	-0.889178
H	3.746544	2.146224	-0.668604
H	2.663086	2.340241	0.748027
H	-0.755677	-1.634030	2.440738
H	0.223869	-0.327753	3.172227
H	0.747809	-2.019195	3.312139
O	-0.096010	1.552754	-1.089984
O	0.496376	1.593089	1.502008
H	-0.163437	3.153465	0.528495
H	-0.262660	1.702344	2.115273
O	-0.950666	3.210408	-0.072873
H	-0.863194	3.882672	-0.783118

4) References

1. A. Company L. Gómez, M. Güell, X. Ribas, J. M. Luis, L. Que, M. Costas *J. Am. Chem. Soc.* **2007,** *129*, 15766-15767.

2. K. Chen, M. Costas, J. Kim, A. K. Tipton, L. Que, Jr. *J. Am. Chem. Soc.* **2002**, *124*, 3026-3035.